

# Semantically Accurate Super-Resolution Generative Adversarial Networks

Tristan Frizza<sup>a</sup>, Donald G. Dansereau<sup>b,\*</sup>, Nagita Mehr Seresht<sup>a</sup>, Michael Bewley<sup>a</sup>

<sup>a</sup>*Nearmap, Level 4 Tower One, International Towers, Barangaroo NSW 2000*

<sup>b</sup>*Australian Centre for Field Robotics, University of Sydney, NSW 2006, Australia*

---

## Abstract

This work addresses the problems of semantic segmentation and image super-resolution by jointly considering the performance of both in training a Generative Adversarial Network (GAN). We propose a novel architecture and domain-specific feature loss, allowing super-resolution to operate as a pre-processing step to increase the performance of downstream computer vision tasks, specifically semantic segmentation. We demonstrate this approach using Nearmap’s aerial imagery dataset which covers hundreds of urban areas at 5-7 cm per pixel resolution. We show the proposed approach improves perceived image quality as well as quantitative segmentation accuracy across all prediction classes, yielding an average accuracy improvement of 11.8% and 108% at 4× and 32× super-resolution, compared with state-of-the-art single-network methods. This work demonstrates that jointly considering image-based and task-specific losses can improve the performance of both, and advances the state-of-the-art in semantic-aware super-resolution of aerial imagery.

*Keywords:* super-resolution, semantic segmentation, generative adversarial networks, multi-modal learning

---

## 1. Introduction

Image super-resolution is a well studied but challenging task in which low-resolution imagery is to be upsampled to a high-fidelity, higher resolution image. While traditional methods draw on decades of image and signal-processing knowledge (Farsiu et al., 2004), these fail to exploit the rich *prior* knowledge we have of what realistic scenes look like. Such knowledge is difficult or impossible to capture by traditional means, but is accessible via learning-based approaches (Anwar et al., 2020), allowing these to achieve much greater levels of fidelity and more aggressive upsampling rates.

Most recently, generative adversarial network (GAN)-based super-resolution architectures (Goodfellow et al.,

2014) have demonstrated state-of-art performance by pairing a generator and adversarial discriminator (Wang et al., 2020). In this scheme, the discriminator learns to distinguish synthetic and captured imagery, while the generator competitively learns to fool it with more realistic generated content.

However, in the context of applications in which semantic meaning is as important as visual realism, GANs risk filling in details that are not semantically faithful. This is of utmost importance in a remote sensing context where we wish to improve resolution without compromising semantic accuracy.

In this work we propose to jointly consider visual and semantic fidelity in training a super-resolution GAN. We show that considering both problems at once improves performance at both, as seen in Fig. 1. The contributions of this work are:

- We present a GAN-based architecture for super-resolving aerial imagery by leveraging semantic label information,

---

\*Corresponding author: Rose St Bldg J04, University of Sydney, Australia

*Email address:* donald.dansereau@sydney.edu.au (Donald G. Dansereau)

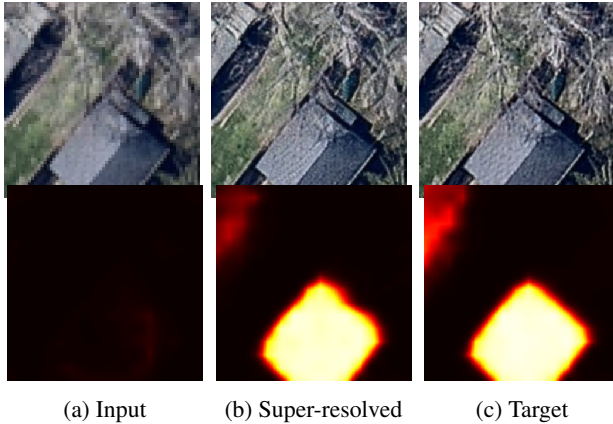


Figure 1: (a) Using conventional segmentation approaches, low-resolution aerial imagery (top) yields poor semantic segmentation predictions (bottom). In this work we present a GAN-based super-resolution strategy that improves both image resolution and semantic segmentation accuracy, yielding results (b) comparable to imagery captured at 4 times the resolution (c).

- We introduce a domain-specific feature loss that jointly optimises detail-oriented perceptual realism as well as semantic accuracy of aerial image features, and
- We demonstrate state-of-the-art super-resolution and improved semantic segmentation of aerial imagery used in an industrial remote sensing application.

This work establishes that a form of multi-modal learning, in which semantics and visual fidelity are jointly addressed, yields superior results at both tasks. We show results for super-resolution in a specific application domain, and anticipate generalisation to both different domains and to applications beyond super-resolution.

The remainder of this paper is organised as follows: in Sec. 2 we review related work and indicate how our relates to what has come before. In Sec. 3 we outline our approach, a novel GAN-based architecture and loss functions that jointly addresses semantic and visual fidelity in super-resolving aerial imagery. Sec. 4 evaluates the method with quantitative and qualitative comparisons to competing methods. Finally, Sec. 5 summarises the work and indicates directions for future work.

## 2. Related Work

This work is concerned with single-image super-resolution. Traditional approaches range in complexity from interpolation (Keys, 1981) to statistical regression with natural image priors (Kim and Kwon, 2010) to sparse coding methods (Yang et al., 2010).

Recently, learning-based methods have demonstrated vastly improved super-resolution performance achieved (Anwar et al., 2020; Saharia et al., 2021). Early applications of neural networks such as SRCNN (Dong et al., 2016) made use of convolutional neural networks (CNNs) to learn non-linear mappings from low to high-resolution image spaces. Later improvements such as VDSR (Kim et al., 2016) saw improved success by increasing network depth. The more recent CNN architectures for super-resolution have shown significant advances by using more sophisticated upsampling strategies, e.g. Laplacian Pyramids (Lai et al., 2018), as well as more efficient layer organisation, e.g. residual (Ledig et al., 2017) and dense (Zhang et al., 2018) network connections.

Innovations in the choice of loss function for image learning tasks have also yielded significant improvements in the fidelity of super-resolution algorithms. Most notable has been the use of so-called perceptual or feature losses (Johnson et al., 2016) that calculate an image loss with respect to the intermediate activations of an auxiliary VGG classification network, rather than a typical mean squared error (MSE) loss on the predicted pixels. This technique yields improved reconstruction of the semantic features of an image, without tending toward blurry, pixel-averaged representations typical of an MSE-based loss.

Most recently, GANs have proven extremely powerful for modelling high-dimensional image data (Goodfellow et al., 2014; Karras et al., 2019; Wang et al., 2020). These pit a generative model against an adversarial discriminator, jointly optimising such that both generation and discrimination improve through training. Their formulation as generative models suits the task of super-resolution well as additional detail must be injected into a low-information image. The main strength of GANs is in their use of a learned loss function, parameterised by a separate loss network which is trained adversarially against the original generator. Models such as SRGAN (Ledig et al., 2017) and ESRGAN (Wang et al., 2018)

have been shown to outperform conventional CNNs in terms of fine texture detail and perceived perceptual similarity.

### 2.1. Super-Resolution in Remote Sensing

Super-resolution has been an increasingly important problem in remote sensing with important applications in environmental monitoring and global change analysis. Accurate identification, localisation and measurement of objects on the ground is a long-running challenge in remote sensing systems. Satellite imaging, while able to scan large areas of the earth’s surface, suffers from low resolution due to imaging from large distances, as well as significant atmospheric distortion. In this work we focus more on high-fidelity overhead aerial imagery that is taken from light aircraft. Rather than spatial resolutions of 30 m typical of LandSat satellite imagery, aerial imaging can reach resolutions in the 5 cm range.

Traditional interpolation, Fourier-domain and Bayesian approaches to super-resolution have found use on aerial imagery (Yang et al., 2015). Among more recent works adopting machine-learning approaches, we highlight the work by Bosch et al. (2018) that achieves impressive results on both satellite and aerial imagery, using DenseNets (Huang et al., 2017) and adversarial learning. However, as the authors note, use of an ImageNet pre-trained network for computing feature matching loss exhibits little correlation between features found in natural and overhead images. Furthermore, the authors acknowledge that their model hallucinates unrealistic detail when approaching higher (8x) upsampling factors, alluding to the fact that this could be improved by including coarse semantic results via a conditional GAN framework.

In this work we address these shortcomings of prior work, using a custom-trained aerial image segmentation model to compute feature loss, imbuing the model with semantically relevant feature comparisons, as well as employing a conditional discriminator that ensures the generated images maintain semantic relevance to the original images, without excessive hallucination. With these enhancements we are able to demonstrate meaningful enhancement of resolution at greater upsampling rates, up to 32x.

### 2.2. Semantic Segmentation in Remote Sensing

Semantic image segmentation involves the dense prediction of image region masks and corresponding classes for each pixel in an image (He et al., 2017). This has seen widespread adoption in autonomous driving and is gaining attention in remote sensing for localising and labelling important ground-level features like vehicles, buildings and other landmarks. Popular models such as FCN (Long et al., 2015), U-Net (Ronneberger et al., 2015) and DeepLab (Chen et al., 2018) have consistently demonstrated the effectiveness of deep neural networks for this task.

Several recent works have demonstrated the benefit of applying super-resolution to improve object classification in aerial images. Shermeyer and Van Etten (2019) successfully combine super-resolution of satellite imagery with SSD (Liu et al., 2016) and YOLO (Redmon et al., 2016) classification networks and report a 13-36% improvement in mean average precision (mAP) for detecting vehicles in their scenes. They however use much coarser resolution imagery than we have available, changing the nature of the problem, and their proposed approach is based on the VDSR network which has been superseded in more recent work. Extensions of this paper (Ferdous et al., 2019) apply GAN models, improving vehicle classification accuracy by super-resolving the input imagery.

In this work we extend these ideas to work on aerial image segmentation, with generalisation to dense labels necessitating high detail and reconstruction accuracy at the pixel level. We improve on prior work by training our GAN super-resolution generator jointly with the segmentation network to optimize for the downstream task, inspired by the improvements of task-driven, end-to-end super-resolution training (Haris et al., 2018).

## 3. Semantically-Aware Super-Resolution

To train a super-resolution network we require pairs of high-resolution images  $x$  and their corresponding low-resolution counterparts  $x'$ . For this we begin with full-resolution images drawn from a practical aerial imagery dataset, and construct from each a low-resolution counterpart using a bilinear downsampling operation with a Gaussian anti-aliasing filter.

Referring to Fig. 2, from these image pairs we learn a function  $G(x')$  approximating the inverse transform from

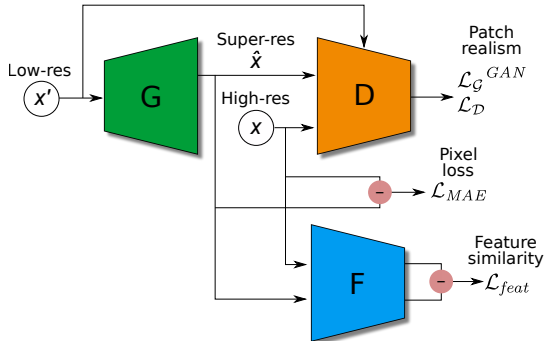


Figure 2: Proposed high-level network architecture: The generator  $G$  learns to create super-resolved images  $\hat{x}$  from low-resolution images  $x'$  based on three losses: the pixel-wise difference between high-resolution and super-resolved signals  $\mathcal{L}_{MAE}$ ; patch realism from the discriminator  $D$  conditioned on  $x'$ ; and feature similarity  $\mathcal{L}_{feat}$  based on the semantically-driven feature embedding  $F$ .

low to high-resolution image space. We then compute a loss based on pixel-wise comparison of the full-resolution and estimated images,  $x$  and  $\hat{x}$ , as well as feedback from a discriminator  $D$  and the quality of the resulting semantic feature mask  $F$ . The choice of loss functions is key to this work and will be covered in depth in Sec. 3.2.

### 3.1. Proposed Network Architecture

Our core network architecture, as illustrated in Fig. 2, is best understood as being composed of 3 networks: a generator, a discriminator, as per a typical GAN formulation, and a pre-trained semantic segmentation network.

The generator is based on the Residual-in-residual Dense Network (RRDN) architecture proposed in ESRGAN (Wang et al., 2018) as we found this offers superior performance over SRResNet and EDSR models. We however opt for a smaller version with 3 dense blocks rather than the original 16 due to the large number of parameters and thus slow training speeds.

For the discriminator (illustrated in Fig. 3) we deviate from a conventional GAN image discriminator. We take inspiration from Pix2Pix (Isola et al., 2017) and employ a patch-based discriminator which outputs predictions over individual “patches” of the input image. This has been shown to outperform standard discriminator formulations which simply output a binary “realness” prediction over

the entire image. We find that it also allows the network to be fully convolutional and thus compatible with arbitrarily sized input images. Furthermore we apply recent work in Spectral Normalisation (Miyato et al., 2018) to scale the weights of the discriminator and guarantee Lipschitz-continuity. We find this to be very important in improving the training stability of GANs since having finitely bounded gradients in the discriminator means that for any generated image, the proposed generator avoids spikes in the backpropagation signal and is less likely to destabilise.

We furthermore modify the discriminator to predict realness of images, conditioned on a nearest-neighbour up-sample of the low-resolution input image (see Fig. 3). This has the benefit of changing the discriminator objective from predicting realistic images standalone to predicting realistic transformation of given source images, which is the true aim of the super-resolution discriminator. This change is also inspired by insight from Isola et al. (Isola et al., 2017), demonstrating that conditioning the discriminator on input images significantly improves pixel accuracy and intersection over union (IoU) scores by penalising generator models with large mismatches between inputs and outputs. This mitigates GAN collapse during training in which the generator can fall into a unimodal state, producing identical outputs regardless of inputs. By maintaining relevance between inputs and outputs, the proposed model can effectively overcome the issue of excessive and unwarranted hallucination of unrealistic detail at higher upsampling factors as is observed in precedent super-resolution works in remote sensing (Bosch et al., 2018).

Finally, we use a domain-specific image segmentation network pre-trained to predict semantic masks over aerial imagery for classes such as cars, roads, vegetation, roofs, solar panels and so on. This network is used in parallel with the discriminator to judge image loss, however it focuses on the reconstruction of semantic image features by comparing the semantic segmentation of the original image to the super-resolved prediction. For this we use the segmentation predictions before thresholding for a probabilistic interpretation. By doing so, we naturally imbue our super-resolution network with specific knowledge of the domain learned separately by the segmentation network. This allows the proposed approach to reconstruct image features that are semantically correct with respect

to the visual task at hand, in this case image segmentation, as well as optimizing for visual fidelity.

### 3.2. Loss Functions

A simple formulation of the loss between two images is the mean across the image of pixel-wise differences, such as the MSE or mean absolute error (MAE). MAE is generally regarded to outperform MSE for super-resolution (Johnson et al., 2016) in that it tends to yield sharper image predictions. We have confirmed these findings and thus adopt the MAE as our pixel loss function:

$$\mathcal{L}_{MAE} = \frac{1}{HWC} \|x - \hat{x}\|_1, \quad (1)$$

where  $H$ ,  $W$ ,  $C$  are the height, width and channel dimensions of the image respectively and  $\hat{x} = G(x')$  is the generator prediction based on our downsampled input image  $x'$ .

The prominent shortcoming of pixel-wise loss functions is that they compute the average loss over all pixels. An unfortunate consequence of this is that models invariably learn to reconstruct images by trying to minimise their average error and hence produce blurry features that are more correct on average. This effectively masks out small-scale variation and hence fine detail in generated images, which is at odds with the goal of super-resolution. Furthermore, a shortfall of pixel-wise losses is that all losses are calculated at the pixel level and hence have no awareness of macroscopic image composition. Thus, we employ two additional loss terms to remedy these issues, the first being a semantic feature loss and the second being a GAN loss.

Feature loss, referred to as perceptual loss by Johnson et al. (2016), was proposed to incorporate the reconstruction of semantic image features by adding a loss term derived from the intermediate activations of an auxiliary classifier network. By feeding both images through this network, the intuition is that if both images have similar semantic content then the classifier activations should be similar. We extend this idea to semantic segmentation networks which produce a spatial mask rather than a single classifier value:

$$\mathcal{L}_{feat} = \frac{1}{HWC} \|F(x) - F(\hat{x})\|_2^2, \quad (2)$$

where  $F(x)$  is the embedding of  $x$  generated by Nearmap’s existing segmentation model pre-trained on high-resolution overhead aerial imagery. We apply the proposed feature loss to train a model to reconstruct important semantic features such as roofing material, roads, etc. Rather than using scalar classification predictions, we calculate the binary cross-entropy loss across predictions on patches of the image, similar to Pix2Pix (Isola et al., 2017).

Finally, we introduce a GAN loss term following the Non-Saturating GAN (NS-GAN) formulation (Goodfellow et al., 2014),

$$\mathcal{L}_G^{GAN} = -\mathbb{E}_{\hat{x} \sim p_g} [\log(D(\hat{x}))], \quad (3)$$

where  $D(x)$  is the discriminator’s estimate of patch realism. We alter the discriminator loss to be conditional on the low-resolution input image,

$$\begin{aligned} \mathcal{L}_D = & -\mathbb{E}_{x \sim p_d} [\log(D(x|x_{nn}))] \\ & -\mathbb{E}_{\hat{x} \sim p_g} [\log(1 - D(\hat{x}|x_{nn}))], \end{aligned} \quad (4)$$

so the discriminator learns not just whether a given high-resolution image is “realistic”, but rather whether it is a realistic super-resolution of a given low-resolution image. We implement this with the nearest-neighbour upsampling of the low-resolution image,  $x_{nn}$ , similar to learning the residual (He et al., 2016).

As is common in combining loss functions (Shen and Stamos, 2020), we employ weighting hyperparameters

$$\mathcal{L}_G = \alpha \mathcal{L}_G^{GAN} + \beta \mathcal{L}_{feat} + \gamma \mathcal{L}_{MAE}, \quad (5)$$

empirically selecting  $\alpha = 1 \times 10^{-3}$ ,  $\beta = 5$  and  $\gamma = 1 \times 10^{-3}$  to achieve a balance between imagined detail and true semantic reconstruction.

## 4. Results

### 4.1. Dataset and Training

For training we use a very large-scale dataset of nearly half a million aerial images accompanied by human annotated feature masks, an example of which is portrayed in Fig. 4. The dataset covers imagery across Australia and the United States, captured at a ground spatial distance (GSD) resolution of 5-7 cm. In this work, we used labels

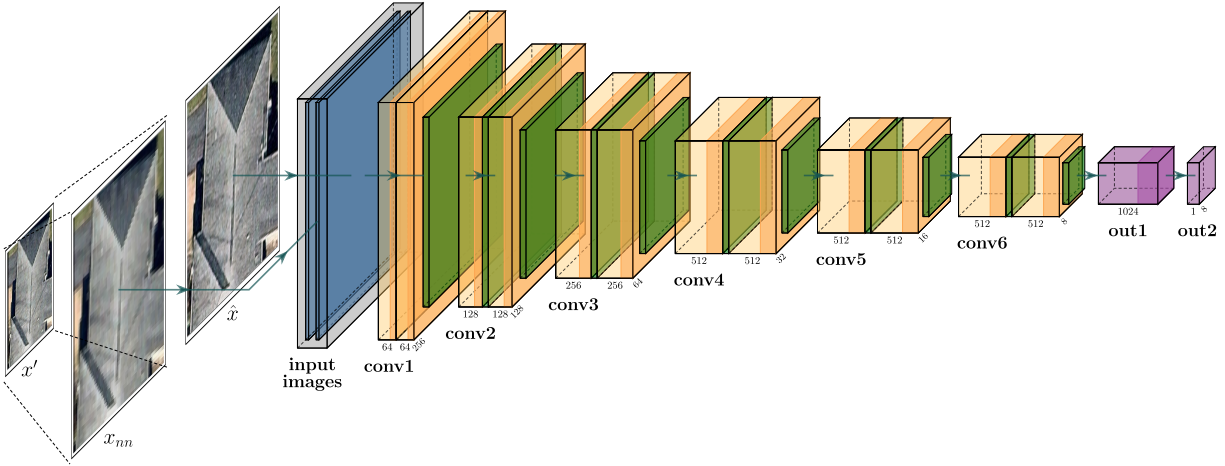


Figure 3: The proposed conditional patch-based discriminator network architecture. Here conv blocks indicate two sets of stacked 3x3 Convolution (yellow) and BatchNorm (green) layers whereas out blocks are single 1x1 Convolutions (purple). Blocks with shaded right hand sides indicate a LeakyReLU activation layer. The low resolution image  $x'$  is nearest-neighbour upsampled to produce  $x_{nm}$  and then concatenated to the generator prediction  $\hat{x}$ .



Figure 4: Typical raster image from dataset, illustrating the predicted segmentation masks for the many landmarks and materials of interest within the scene. For more information visit the Nearmap AI Documentation <https://docs.nearmap.com/display/ND/NEARMAP+AI>.

for 34 unique categories of typical aerial image features including specific object instances (swimming pool, solar panel), materials (shingle roof, tile roof), and other common features (water body, shadow).

We trained our super-resolution models using TensorFlow 2 on an NVIDIA V100 GPU, using a batch size of 16. We employed a two-stage training procedure of first

performing supervised pre-training of the generator with an MAE pixel-wise loss (Eq. 1), then fine-tuned with the discriminator network in an adversarial scenario. This approach significantly accelerated convergence and helped avoid instability characteristic of GAN models in early iterations of training.

We employed the ADAM optimiser (Kingma and Ba, 2014), using a pre-training learning rate of  $lr_g = 2 \times 10^{-4}$ . For fine-tuning we employed different initial learning rates for the generator and discriminator networks, starting at  $lr_g = 1 \times 10^{-4}$  and  $lr_d = 2 \times 10^{-4}$  respectively. We found that decaying these by a factor of one half every 10,000 optimizer steps yielded reliable GAN convergence. Typically we trained for between 10,000 and 40,000 iterations with longer training required for the higher upsampling factors. Further training showed a regression in quality associated with over-fitting.

To accelerate training and performance at higher upsampling rates, we initialised the model with weights trained for lower upsampling rates. This is consistent with previous works showing super-resolution models benefit from information learned at multiple scales (Lim et al., 2017), and leave the exploration of multi-scale architectures for future work.

#### 4.2. Image Quality Metrics

To evaluate image quality we employ three well-known full-reference image metrics: Peak signal-to-noise ratio (PSNR) measured in dB as

$$\text{PSNR} = 10 \cdot \log_{10} \left( \frac{\text{MAX}_I^2}{\text{MSE}} \right), \quad (6)$$

where  $\text{MAX}_I$  is the maximum pixel intensity in the image and MSE is the mean-squared error.

Structural similarity index (SSIM), designed to more closely reflect subjective evaluation of image fidelity:

$$\text{SSIM}(x, y) = \frac{(2\mu_x\mu_y + c_1)(2\sigma_{xy} + c_2)}{(\mu_x^2 + \mu_y^2 + c_1)(\sigma_x^2 + \sigma_y^2 + c_2)}, \quad (7)$$

where  $\mu$  and  $\sigma$  are the mean and standard deviation of their respective images and  $c_1, c_2$  are constants proportional to the dynamic range of the given images.

And finally multi-scale structural similarity index (MS-SSIM), which extends SSIM as a weighted average at various downsampled resolutions. The latter is often reported for super-resolution tasks as these deal with judging image quality over several scales. We employed the implementations of these metrics found in Tensorflow’s image module<sup>1</sup>.

#### 4.3. Image Segmentation Metrics

One of the most commonly used metrics in semantic segmentation is the IoU, also referred to as the Jaccard Index. It compares predicted and known target masks  $A$  and  $B$  by taking the ratio

$$\text{IoU}(A, B) = \frac{|A \cap B|}{|A \cup B|}. \quad (8)$$

Since we aim to improve segmentation accuracy over a multi-class dataset, we report the class-wise mean intersection over union (mIoU), taken as the mean IoU over label classes (Long et al., 2015).

We also report the percentage improvement of the proposed method  $A$  relative to a baseline method  $B$  as

$$\% \text{Improvement}(A, B) = \frac{A - B}{B} \cdot 100. \quad (9)$$

Table 1: A comparison of three potential generator model architectures for 4× super-resolution. We chose RRDN for all subsequent experiments due to its superior overall performance on pixel-wise loss objectives.

Model	MAE Loss	PSNR	SSIM	MS-SSIM
SRResNet	0.04066	25.44	0.6919	0.9296
EDSR	0.04059	25.45	0.6930	0.9301
RRDN	<b>0.04035</b>	<b>25.51</b>	<b>0.6957</b>	<b>0.9308</b>

#### 4.4. Super-Resolution Performance

To select a generator model architecture, we compared four alternatives for 4× super-resolution using only a pixel-wise loss objective. Results are summarized in Table 1, showing that the RRDN-style backbone performed best at this task.

We compared our approach to bilinear upsampling and RRDN, with typical results depicted in Fig. 5. Although not always quantitatively superior, images produced by the proposed GAN-based approach are of superior perceptual quality, most notably in reconstruction of detail and texture. An additional detailed example is shown in Fig. 6. It is understood that simple image metrics like PSNR and SSIM do not necessarily reflect qualitative fidelity (Ledig et al., 2017; Wang et al., 2018), limiting their utility in assessing GAN performance.

#### 4.5. Semantic Segmentation Performance

We compared semantic segmentation masks derived from the low-resolution images, their high-resolution counterparts, and from upsampled images generated by the GAN-based super-resolution models trained in the previous section. Qualitative and quantitative results are depicted in Fig. 5. Masks derived from the low-resolution imagery are either very poor or non-existent, while upsampled imagery show significant improvement. The proposed GAN provided the best performance, outperforming generator-only CNN models (i.e. RRDN) due to its ability to augment finer detail and textural patterns. This is clearest in Figs. 5j and 5k, with the latter showing dramatically improved IoU compared with RRDN, increasing from 0 to 0.96 due to the generation of realistic tree

<sup>1</sup>[www.tensorflow.org/api\\_docs/python/tf/image](http://www.tensorflow.org/api_docs/python/tf/image)



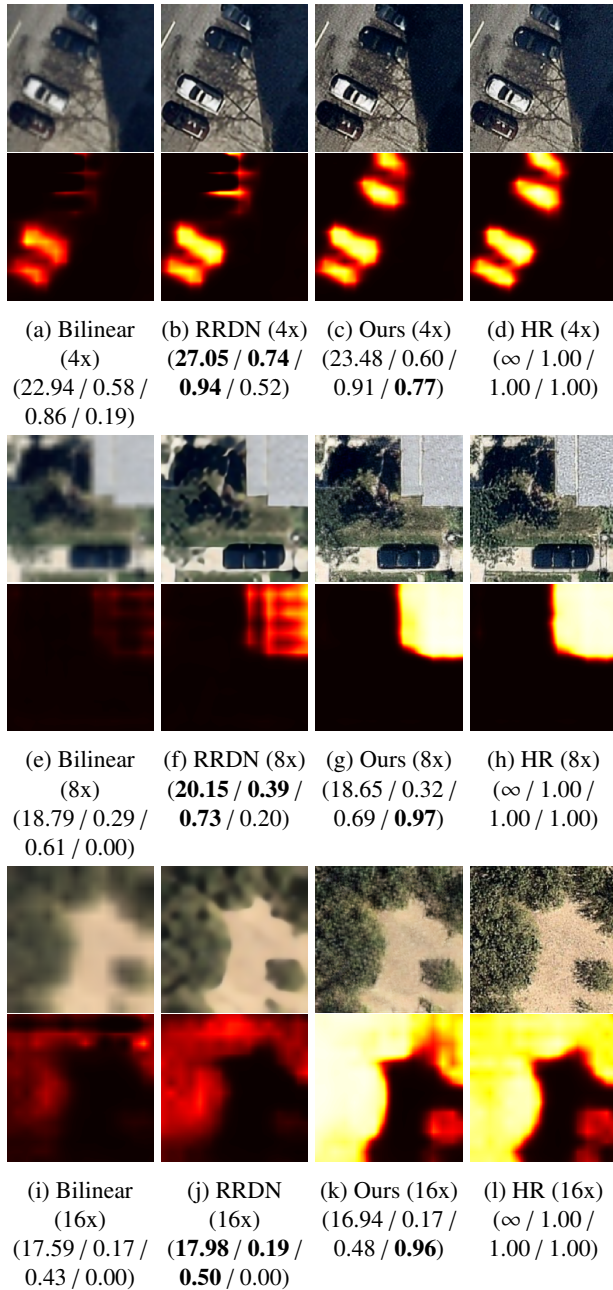


Figure 5: Comparison of image super-resolution and semantic mask performance. We compare naïve bilinear upsampling, the state-of-the-art CNN-based RRDN, the proposed GAN approach, and the original high-resolution (HR) target image across four upsampling rates. For each example we report the PSNR, SSIM, MS-SSIM and IoU respectively. The proposed method shows the strongest perceptual fidelity and segmentation performance.

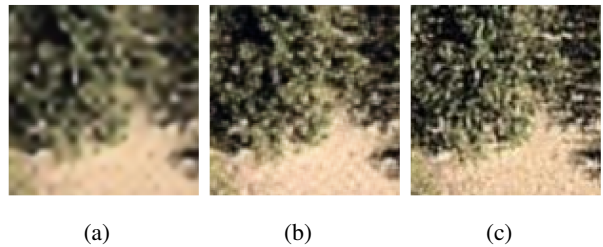


Figure 6: Detailed close-up of super-resolved imagery generated with (a) a CNN trained with PSNR-based loss, (b) the proposed GAN, and (c) the ground-truth original image. PSNR tries to maximise accuracy on average over pixels causing blurry reconstructions, whereas the GAN is penalised for not recovering fine detail and hence learns to generate high-frequency textures.

foliage patterning which is clearly a crucial feature for the segmentation network. Note also that the semantic segmentation performance with the proposed method is very similar to performance using the ground-truth high-resolution images.

Table 2 summarizes a comparison of semantic segmentation performance across the entire test set, for four upsampling factors. Each experiment starts with the same high-resolution images, then downsamples these by the specified factor. The  $32\times$  results are dealing with much less informative imagery than the the  $4\times$  imagery, explaining the lower absolute performance at higher upsampling rates.

The results show the proposed method significantly outperforming the baseline bilinear upsampling, and the CNN-based RRDN, with the performance margin widening for greater upsampling rates. At lower upsampling rates the proposed method yields an improvement of 11.8% in mIoU compared with the CNN-based method. At these scales the low-resolution images still contain sufficient detail that a CNN can essentially perform image sharpening to yield reasonable results. However, for higher upsampling rates image sharpening fails, and image segmentation performance for CNN-based methods is poor. The GAN-based methodology reconstructs textural detail, yielding a 108% improvement in IoU over RRDN.

#### 4.6. Class-Wise Analysis

To better understand the performance of each method, we compared the proposed approach with the CNN-based



RRDN across individual semantic classes, for a conservative upsampling factor of  $4\times$ . The results are depicted in Fig. 7, showing the proposed model outperforms RRDN in 27 out of 29 categories, with up to an 86.0% improvement seen in the Construction Site class, and only small regressions in its weakest classes.

The proposed approach provides the strongest advantage when resolving finely textured classes, e.g. roofing (Tile Roof 52.0%, Shingle Roof 20.3% and Metal Roof 14.4%) and vegetation (Very Low Vegetation 35.9% and Medium-High Vegetation 26.0%). The proposed method’s use of both pixel-level and semantic fidelity allows it to infer and retain relevant textural detail.

Similarly, the proposed method shows less of an advantage for categories with little textural detail, e.g. Asphalt and Shadow, and outline-oriented categories like roof shape (Dutch Gable, Gable, Hip Roofs). We expect these trends to be amplified for higher upsampling rates, following the results in Table 2.

## 5. Conclusion and Future Work

We have demonstrated the benefits of super-resolution image enhancement for improving semantic segmentation performance in remote sensing applications. We proposed an end-to-end GAN-based framework that jointly optimised for image fidelity and semantic feature reconstruction, showing improved performance at both tasks. The proposed method significantly outperforms traditional and state-of-the-art CNN methods, both of which suffer from loss of texture and poor feature reconstruction. We achieved up to a 108% improvement in IoU compared

Table 2: Comparison of mIoU averaged across all classes. mIoU for the original high-resolution images is 0.543 and represents an upper bound on performance. Relative percentage improvement (Eq. 9) shows substantial improvement in the proposed GAN results compared with the CNN-based approach.

Scale	Bilinear	CNN	GAN (ours)	% Improvement
4x	0.389	0.468	<b>0.523</b>	11.8
8x	0.187	0.368	<b>0.481</b>	30.7
16x	0.095	0.212	<b>0.388</b>	83.0
32x	0.068	0.120	<b>0.250</b>	108

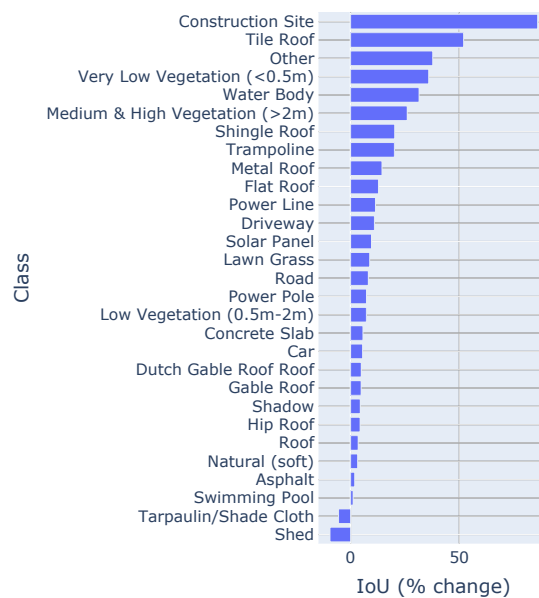


Figure 7: Percentage improvement (Eq. 9) of class-wise mIoU between our GAN approach and CNN upsampling at  $4\times$  super-resolution. The proposed approach shows substantial performance gains of up to 86.0%, showing the strongest improvement for classes with fine textural detail.

with a leading CNN-based method, pushing our achievable resolution factor as far as 32x whilst retaining meaningful results.

This work advances deep learning-based image processing as a means of overcoming expensive and challenging hardware constraints in practical aerial imaging applications. As future work we envision jointly learning additional semantically meaningful tasks, and incorporating multiple views into semantically aware super-resolution.

## References

- Anwar, S., Khan, S., Barnes, N., 2020. A deep journey into super-resolution: A survey. *ACM Computing Surveys (CSUR)* 53, 1–34.
- Bosch, M., Gifford, C.M., Rodriguez, P.A., 2018. Super-resolution for overhead imagery using densenets and adversarial learning, in: *IEEE Winter Conference on Applications of Computer Vision (WACV)*, IEEE. pp. 1414–1422.
- Chen, L.C., Zhu, Y., Papandreou, G., Schroff, F., Adam, H., 2018. Encoder-decoder with atrous separable convolution for semantic image segmentation, in: *Proceedings of the European conference on computer vision (ECCV)*, pp. 801–818.
- Dong, C., Loy, C., He, K., Tang, X., 2016. Image super-resolution using deep convolutional networks. *IEEE Transactions on Pattern Analysis and Machine Intelligence (TPAMI)* 38, 295–307.
- Farsiu, S., Robinson, D., Elad, M., Milanfar, P., 2004. Advances and challenges in super-resolution. *International Journal of Imaging Systems and Technology* 14, 47–57.
- Ferdous, S.N., Mostofa, M., Nasrabadi, N.M., 2019. Super resolution-assisted deep aerial vehicle detection, in: *Artificial Intelligence and Machine Learning for Multi-Domain Operations Applications*, International Society for Optics and Photonics. p. 1100617.
- Goodfellow, I., Pouget-Abadie, J., Mirza, M., Xu, B., Warde-Farley, D., Ozair, S., Courville, A., Bengio, Y., 2014. Generative adversarial nets. *Advances in neural information processing systems* 27.
- Haris, M., Shakhnarovich, G., Ukita, N., 2018. Task-driven super resolution: Object detection in low-resolution images. *arXiv preprint 1803.11316*.
- He, K., Gkioxari, G., Dollár, P., Girshick, R., 2017. Mask R-CNN, in: *International Conference on Computer Vision (ICCV)*, pp. 2961–2969.
- He, K., Zhang, X., Ren, S., Sun, J., 2016. Deep residual learning for image recognition, in: *Computer Vision and Pattern Recognition (CVPR)*, IEEE Computer Society. pp. 770–778.
- Huang, G., Liu, Z., Van Der Maaten, L., Weinberger, K.Q., 2017. Densely connected convolutional networks, in: *Computer Vision and Pattern Recognition (CVPR)*, IEEE. pp. 2261–2269.
- Isola, P., Zhu, J.Y., Zhou, T., Efros, A.A., 2017. Image-to-image translation with conditional adversarial networks, in: *Computer Vision and Pattern Recognition (CVPR)*, pp. 5967–5976.
- Johnson, J., Alahi, A., Fei-Fei, L., 2016. Perceptual losses for real-time style transfer and super-resolution, in: *European conference on computer vision (ECCV)*, Springer. pp. 694–711.
- Karras, T., Laine, S., Aila, T., 2019. A style-based generator architecture for generative adversarial networks, in: *Computer Vision and Pattern Recognition (CVPR)*, pp. 4401–4410.
- Keys, R.G., 1981. Cubic Convolution Interpolation for Digital Image Processing. *IEEE Transactions on Acoustics, Speech, and Signal Processing* 29, 1153–1160. doi:10.1109/TASSP.1981.1163711.
- Kim, J., Lee, J.K., Lee, K.M., 2016. Accurate image super-resolution using very deep convolutional networks, in: *Computer Vision and Pattern Recognition (CVPR)*, pp. 1646–1654. doi:10.1109/CVPR.2016.182.
- Kim, K.I., Kwon, Y., 2010. Single-image super-resolution using sparse regression and natural image prior. *Transactions on Pattern Analysis and Machine Intelligence*

- (TPAMI) 32, 1127–1133. doi:10.1109/TPAMI.2010.25.
- Kingma, D.P., Ba, J., 2014. ADAM: A method for stochastic optimization. arXiv preprint arXiv:1412.6980 .
- Lai, W.S., Huang, J.B., Ahuja, N., Yang, M.H., 2018. Fast and accurate image super-resolution with deep laplacian pyramid networks. *IEEE Transactions on Pattern Analysis and Machine Intelligence (TPAMI)* 41, 2599–2613.
- Ledig, C., Theis, L., Huszár, F., Caballero, J., Cunningham, A., Acosta, A., Aitken, A., Tejani, A., Totz, J., Wang, Z., Shi, W., 2017. Photo-realistic single image super-resolution using a generative adversarial network, in: *Computer Vision and Pattern Recognition (CVPR)*, pp. 105–114.
- Lim, B., Son, S., Kim, H., Nah, S., Lee, K.M., 2017. Enhanced Deep Residual Networks for Single Image Super-Resolution, in: *Computer Vision and Pattern Recognition (CVPR) Workshops*, pp. 1132–1140.
- Liu, W., Anguelov, D., Erhan, D., Szegedy, C., Reed, S., Fu, C.Y., Berg, A.C., 2016. SSD: Single shot multibox detector, in: *European Conference on Computer Vision (ECCV)*, Springer. pp. 21–37.
- Long, J., Shelhamer, E., Darrell, T., 2015. Fully convolutional networks for semantic segmentation, in: *Computer Vision and Pattern Recognition (CVPR)*, pp. 3431–3440.
- Miyato, T., Kataoka, T., Koyama, M., Yoshida, Y., 2018. Spectral normalization for generative adversarial networks, in: *International Conference on Learning Representations*.
- Redmon, J., Divvala, S., Girshick, R., Farhadi, A., 2016. You only look once: Unified, real-time object detection, in: *Computer Vision and Pattern Recognition (CVPR)*, pp. 779–788.
- Ronneberger, O., Fischer, P., Brox, T., 2015. U-Net: Convolutional networks for biomedical image segmentation, in: *International Conference on Medical image computing and computer-assisted intervention*, Springer. pp. 234–241.
- Saharia, C., Ho, J., Chan, W., Salimans, T., Fleet, D.J., Norouzi, M., 2021. Image super-resolution via iterative refinement. arXiv preprint arXiv:2104.07636 .
- Shen, X., Stamos, I., 2020. Frustum voxnet for 3D object detection from RGB-D or depth images, in: *Winter Conference on Applications of Computer Vision (WACV)*, pp. 1698–1706.
- Shermeyer, J., Van Etten, A., 2019. The effects of super-resolution on object detection performance in satellite imagery, in: *Computer Vision and Pattern Recognition (CVPR) Workshops*.
- Wang, X., Yu, K., Wu, S., Gu, J., Liu, Y., Dong, C., Qiao, Y., Change Loy, C., 2018. ESRGAN: Enhanced super-resolution generative adversarial networks, in: *Proceedings of the European Conference on Computer Vision (ECCV) workshops*.
- Wang, Z., Jiang, K., Yi, P., Han, Z., He, Z., 2020. Ultra-dense gan for satellite imagery super-resolution. *Neurocomputing* 398, 328–337.
- Yang, D., Li, Z., Xia, Y., Chen, Z., 2015. Remote sensing image super-resolution: Challenges and approaches, in: *2015 IEEE International Conference on Digital Signal Processing (DSP)*, pp. 196–200.
- Yang, J., Wright, J., Huang, T., Ma, Y., 2010. Image super-resolution via sparse representation. *IEEE Transactions on Image Processing (TIP)* 19, 2861–2873.
- Zhang, Y., Tian, Y., Kong, Y., Zhong, B., Fu, Y., 2018. Residual dense network for image super-resolution, in: *Computer Vision and Pattern Recognition (CVPR)*, pp. 2472–2481.